JOURNAL OF MATERIALS SCIENCE 30 (1995) 3024–3032

Stress transfer in the fibre fragmentation test

Part II *Multiple fibre composites*

J. K. KIM*
Department of Engineering, Faculty of Engineering and Information Technology, Australian National University, Canberra, ACT 0200, Australia

Y. W. MAI
Centre for Advanced Materials Technology, Department of Mechanical and Mechatronics Engineering, University of Sydney, Sydney, NSW 2006, Australia

The micromechanics of stress transfer has been analysed in a multiple-fibre composite which was subjected to uniaxial tension. The model composite was treated as a three-cylinder assemblage, which consisted of a central fibre, a matrix annulus and a composite medium. Analytical solutions have been derived for all major stress components for the composite with fully bonded fibre–matrix interface. A parametric study was performed on a carbon fibre–epoxy matrix composite. The result suggests that the principal effect of a stiff composite medium surrounding a discontinuous isolated fibre due to the high fibre volume fraction and stiff matrix, is to reduce the efficiency of stress transfer over the central potion of the fibre, while promoting the fibre–matrix interface shear stress concentration at the fibre end region. Practical implications of this observation with respect to fibre fragmentation and interfacial debonding are discussed.

1. Introduction

The fibre fragmentation test [1] has now become one of the most important microcomposite test methods developed as a means of evaluating the bond quality at the fibre–matrix interface [2]. A critical review [3] has recently been presented of theoretical aspects of this test method with a particular emphasis on the statistical nature of the fibre fragmentation process and the interface debonding phenomenon. Because the stress fields and the damage process arising in this test closely resemble those of many composite components in service conditions, a fundamental understanding of this knowledge is essential to the design of practical fibre composites of load-bearing nature [4]. Since the advent of the shear lag model [5], this loading geometry has been most widely used for theoretical analyses of fibre composites in order to understand the efficiency of the stress transfer across the interface.

From both the stress transfer and fracture mechanics viewpoints, an improved micromechanics model of the single-fibre fragmentation test was presented in Part I of this paper [6]. Interfacial debonding was analysed based on the shear strength criterion in which the debond crack propagates when the maximum interfacial shear stress at the fibre ends reaches the shear strength of the interface. It was assumed that the fibre breaks when the maximum fibre axial stress taking place at the fibre centre exceeds the average tensile strength based on Weibull statistics. Depending on the interface properties and the fibre tensile strength for given elastic constants of the composite constituents, three distinct conditions for the interface can be identified, namely full bonding, partial debonding and full frictional bonding. The specific criteria necessary to satisfy each interface condition were also properly quantified. In a parametric study employing a model composite of carbon fibre–epoxy matrix, a characteristic applied stress can be identified, below which no debonding takes place. With increasing applied stress from this value the debond length increases towards a plateau value. The mean fibre fragmentation length can be predicted, which is the sum of the debond and bond lengths.

As a continuation of the previous study, the theoretical analysis of the fibre fragmentation test geometry was further extended for composites containing fibres of high volume fraction. A particular emphasis was placed on examining the effects of the interactions between neighbouring fibres and the fibre volume fraction on the stress transfer in a single broken fibre segment. For this purpose, the multiple fibre composite was treated as a three-cylinder model which consisted of three coaxially located components, namely a circular fibre, a matrix annulus and a composite medium. The first two are the elements of the single-fibre composite, while the composite medium represents a homogeneous trans-isotropic assemblage

* Present address: Department of Mechanical Engineering, Hong Kong University of Science and Technology, Clear Water Bay, Hong Kong.

0022–2461

of fibres and matrix material with its fibre volume fraction being identical to the core single-fibre composite. The three-cylinder composite model has been successfully applied to the analysis of fibre pull-out test on composites with and without an interfacial coating [7–9].

2. Theoretical analysis

2.1. Basic governing conditions

The three-cylinder composite model shown in Fig. 1 contains a single discontinuous fibre of length $2L$ embedded at the centre of a coaxial cylindrical shell of matrix which, in turn, is surrounded by a trans-isotropic composite medium. The radii of the elements are a, b and B, respectively. The tensile stress in the composite medium at $z = \pm L$, $\sigma = \sigma_a B^2/(B^2 - b^2)$, is caused by the external stress, σ_a, applied to the composite medium at its remote ends. The external stress is transferred to the matrix across the matrix–composite interface which, in turn, is transferred to the fibre across the fibre–matrix interface.

A set of cylindrical coordinates (r, θ, z) is selected for the analysis such that the z-axis corresponds to the axis of the fibre. The mode of deformation is assumed symmetric about the fibre axis as well as about the plane perpendicular to the centre of the fibre at $z = 0$. Therefore, the stress components $(\sigma^r, \sigma^\theta, \sigma^z, \tau^{rz})$ and the displacement components (u^r, u^z) are all independent of the tangential coordinate, θ. The remaining stress and displacement components are zero. Following the previous analysis [6], it is assumed that the cross-section of the fibre ends is separated from the composite so that no stress is transferred through the fibre ends (i.e. $\sigma_f^z = 0$ at $z = \pm L$). Fully bonded interface is considered for the whole fibre length in the present paper.

2.2. Solutions for the stress components

For the cylindrical coordinate of the three-cylinder composite, the basic governing equations and the mechanical equilibrium conditions are basically similar to those employed for the single-fibre composite [6]. For perfectly elastic and isotropic fibre and matrix, and elastic trans-isotropic composite medium, the axial stresses, $\sigma_f^z(z)$, $\sigma_m^z(r, z)$ and $\sigma_c^z(z)$, and the shear stresses, $\tau_m(r, z)$ and $\tau_c(r, z)$, are related to the displacements by

$$\frac{\partial u_f^z(z)}{\partial z} = \frac{1}{E_f}\{\sigma_f^z(z) - \nu_f[\sigma_f^r(r), z + \sigma_f^\theta(r, z)]\} \quad (1)$$

$$\frac{\partial u_m^z(z)}{\partial z} = \frac{1}{E_m}\{\sigma_m^z(z) - \nu_m[\sigma_m^r(r, z) + \sigma_m^\theta(r, z)]\} \quad (2)$$

$$\frac{\partial u_c^z(z)}{\partial z} = \frac{1}{E_c}\{\sigma_c^z(z) - \nu_c[\sigma_c^r(r, z) + \sigma_c^\theta(r, z)]\} \quad (3)$$

$$\frac{\partial u_m^z(r, z)}{\partial r} = \frac{2(1 + \nu_m)}{E_m}\tau_m(r, z) \quad (4)$$

$$\frac{\partial u_c^z(r, z)}{\partial r} = \frac{2(1 + \nu_c)}{E_c}\tau_c(r, z) \quad (5)$$

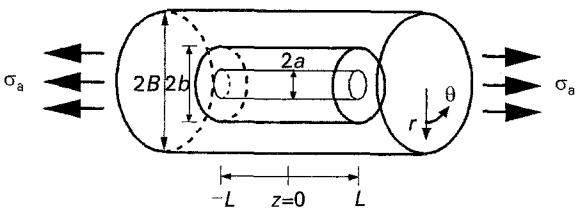

Figure 1 A schematic drawing of a three-cylinder composite in the fibre fragmentation model.

where the subscripts f, m and c refer to fibre, matrix and composite, respectively while the superscripts are coordinate directions. E and ν are Young's modulus and Poisson's ratio, respectively. For a thin fibre, the axial displacement is assumed independent of the radial position. The stress components in the radial and circumferential directions are small compared to the axial stress components, and thus are neglected in Equations 1–3. For the shear strains in the matrix and composite medium in Equations 4 and 5, the radial displacement gradient with respect to the axial direction is neglected as compared to the axial displacement gradient with respect to the radial direction. For the trans-isotropic composite medium, E_c and ν_c in Equations 3 and 5 can be approximated, based on the simple rule of mixtures in the axial direction

$$E_c = E_f V_f + E_m(1 - V_f) \quad (6a)$$

$$\nu_c = \nu_f V_f + \nu_m(1 - V_f) \quad (6b)$$

where $V_f = (a/b)^2$ is the volume fraction of fibre in the core single-fibre composite, which is identical to that in the composite medium. The simple rule of mixtures given in Equation (6a and b) is only valid provided the aspect ratio of the fibre, L/a, is maintained sufficiently large so that the Young's modulus of the composite medium, E_c, is little affected by the instantaneous fibre length. The mechanical equilibrium between the tensile stress, σ, and the internal stress distributions in the composite constituents requires that

$$B^2\sigma = a^2\sigma_f^z(z) + 2\int_a^b r\sigma_m^z(r, z)\,dr + 2\int_b^B r\sigma_c^z(r, z)\,dr \quad (7)$$

The external stress applied to the composite medium is transferred to the matrix through the matrix–composite interfacial shear stress, $\tau_i(b, z)$, which in turn, is transferred to the fibre through the fibre–matrix interfacial shear stress, $\tau_i(a, z)$, such that

$$\frac{d\sigma_f^z(z)}{dz} = -\frac{2}{a}\tau_f(a, z) \quad (8)$$

$$\frac{d}{dz}\left[\int_a^b r\sigma_m^z(r, z)\right] = a\tau_i(a, z) + b\tau_i(b, z) \quad (9)$$

Shear stresses in the matrix, $\tau_m(r, z)$, and in the composite medium, $\tau_c(r, z)$, have the Lamè form [10]

$$\tau(r, z) = P_1 r + \frac{P_2}{r} \quad (10)$$

where P_1 and P_2 are functions of z. For the boundary conditions at the interfaces between the composite constituents, i.e. $\tau_m(a, z) = \tau_i(a, z)$ at $r = a$,

$\tau_m(b, z) = \tau_c(b, z) = \tau_i(b, z)$ at $r = b$, $\tau_c(c, z) = 0$ at $r = c$, the shear stresses $\tau_m(a, z)$ and $\tau_c(b, z)$ are given as a function of the interface shear stresses, $\tau_i(a, z)$ and $\tau_i(b, z)$

$$\tau_m(r, z) = \frac{\gamma}{a^2}\left\{[b\tau_i(b, z) - a\tau_i(a, z)]r + \frac{ab[b\tau_r(b, z) - a\tau_i(a, z)]}{r}\right\} \quad (11)$$

$$\tau_c(r, z) = \gamma_1 \frac{B^2 - r^2}{br}\tau_i(b, z) \quad (12)$$

where the volume ratios between the composite constituents are $\gamma = a^2/(b^2 - a^2)$ and $\gamma_1 = b^2/(B^2 - b^2)$. For the matrix annulus ($a \leqslant r \leqslant b$), combination of Equations 2, 4 and 11 for the axial displacement continuity at the fibre–matrix interface (i.e. $u_m^z(a, z) = u_f^z(z)$) and integration gives

$$\tau_m(r, z) = \frac{1}{a^2 S_2}\left(\frac{b^2}{r} - r\right)\frac{E_m[U_m(b, z) - U_f(z)]}{2(1 + \nu_m)} + \left(\frac{b\gamma}{a^2}\right)\left[\left(\frac{s_1}{s_2}\right)\left(\frac{b^2}{r} - r\right) - \left(\frac{a^2}{r} - r\right)\right]\tau_i(b, z) \quad (13)$$

$$\tau_i(a, z) = \frac{E_m[u_m(b, z) - u_f(z)]}{2a\gamma s_2(1 + \nu_m)} + \left(\frac{b}{a}\right)\left(\frac{s_1}{s_2}\right)\tau_i(b, z) \quad (14)$$

where the non-dimensional coefficients s_1 and s_2 are given in Appendix 1. The matrix axial stress can be derived based on the relations between the stress components and the axial displacements given in Equations 1, 2, 4 and 13.

$$\sigma_m^z(r, z) = \sigma_m^z(a, z) + \frac{\left[b^2\ln(r/a) - \frac{(r^2 - a^2)}{2}\right]\left[\sigma_m^z(b, z) - \sigma_m^z(a, z)\right]}{a^2 s_2} + \frac{2b\gamma(1 + \nu_m)}{a^2}\frac{d\tau_i(b, z)}{dz}\left\{\left(\frac{s_1}{s_2}\right)\left[b^2\ln(r/a) - \frac{(r^2 - a^2)}{2}\right] - \left[a^2\ln\left(\frac{r}{a}\right) - \frac{(r^2 - a^2)}{2}\right]\right\} \quad (15)$$

where $\sigma_m^z(a, z)(= \alpha\sigma_f^z(z))$ and $\sigma_m^z(b, z)$ are the matrix axial stresses at the interfaces $r = a$ and $r = b$, respectively. $\alpha(= E_m/E_f)$ is the Young's modulus ratio of the matrix to the fibre.

Similarly, the stress components can be derived for the composite medium ($b \leqslant r \leqslant B$). Combining Equations 3, 5 and 12 for the axial displacement continuity at the matrix–composite interface (i.e. $u_m^z(b, z) = u_c^z(b, z)$ at $r = b$) and integration gives

$$\tau_c(r, z) = \frac{E_c[u_c(B, z) - u_c(b, z)]}{2b^2 s_5(1 + \nu_c)}\left(\frac{B^2}{r} - r\right) \quad (16)$$

$$\tau_i(b, z) = \frac{E_c[u_c(c, z) - u_c(b, z)]}{2b\gamma_1 s_5(1 + \nu_c)} \quad (17)$$

where the non-dimensional coefficients s_5, are given in Appendix 1. Therefore, the composite axial stress is derived from Equations 3, 5, 12 and 17

$$\sigma_c^z(r, z) = \sigma_c^z(b, z) + \frac{\left[B^2\ln(r/b) - \frac{(r^2 - b^2)}{2}\right][\sigma_c^z(B, z) - \sigma_c^z(b, z)]}{b^2 s_5} \quad (18)$$

where $\sigma_c^z(b, z)$ $(= \sigma_m^z(b, z)/\alpha_1)$ and $\sigma_c^z(B, z)$ are the composite axial stresses at the interfaces, $r = a$ and $r = b$, respectively. $\alpha_1(= E_m/E_c)$ is the Young's modulus ratio of the matrix to the composite. Having determined the stress components in the matrix and the composite medium, combination of Equations 14, 15, 17 and 18 with the mechanical equilibrium Equation 7 yields

$$\sigma_c^z(B, z) = \frac{-a^2\gamma_1 s_2 s_5(1 + \nu_c)}{s_1}\frac{d^2\sigma_f^z(z)}{dz^2} + \frac{\alpha\gamma_1 s_5(1 + \nu_c)}{\gamma s_1(1 + \nu_m)}\sigma_f^z(z) + \frac{\gamma s_1(1 + \nu_m) - \alpha_1\gamma_1 s_5(1 + \nu_c)}{\alpha_1\gamma s_1(1 + \nu_m)}\sigma_m^z(b, z) \quad (19)$$

$$\sigma_m^z(b, z) = \left\{a^2\Big/\left[\frac{s_3}{s_1} + \left(\frac{b}{a}\right)^2 T_4\right]\right\} \times \left\{\left[\left(\frac{b}{a}\right)^2 T_2 - T_1\right]\frac{d^2\sigma_f^z(z)}{dz^2} - \left[1 + \frac{s_3}{s_1} + \left(\frac{b}{a}\right)^2 T_3\right]\sigma_f^z(z) + \left(\frac{B}{a}\right)^2\sigma\right\} \quad (20)$$

where the non-dimensional coefficients s_3, T_1, T_2, T_3 and T_4 are given in Appendix 1. Combining Equations 8, 9, 19 and 20 yields a fourth order differential equation for the fibre axial stress as

$$\frac{a^4 d^4\sigma_f^z(z)}{dz^4} + a^2 Q_1\frac{d^2\sigma_f^z(z)}{dz^2} + Q_2\sigma_f^z(z) - Q_2 Q_3\sigma = 0 \quad (21)$$

where the coefficients Q_1, Q_2 and Q_3 are given in Appendix 1. The general solution of $\sigma_f^z(z)$ in Equation 21 has the form

$$\sigma_f^z(z) = Q_3\sigma + R_1\exp(\beta_3 z) + R_2\exp(-\beta_3 z) \quad (22)$$

where the coefficient β_3 is a function of the elastic properties and the geometric factors of the composite constituents and is given by

$$\beta_3^2 = \frac{1}{2a^2}[-Q_1 + (Q_1^2 - 4Q_2]^{1/2}] \quad (23)$$

R_1 and R_2 in Equation 22 are determined for the boundary condition of an unbonded cross-section at both ends of the fibre, i.e. $\sigma_f^z(z) = 0$ at $z = \pm L$. Thus

$$R_1 = R_2 = \frac{-Q_3\sigma}{2\cosh(\beta_3 L)} \tag{24}$$

Therefore, the solutions for the axial stresses, $\sigma_f^z(z)$, $\sigma_m^z(r, z)$ and $\sigma_c^z(r, z)$ in the composite constituents, which are normalized with the remotely applied stress, σ_a, are given as

$$\frac{\sigma_f^z(z)}{\sigma_a} = (1 + \gamma_1)Q_3\left[1 - \frac{\cosh(\beta_3 z)}{\cosh(\beta_3 L)}\right] \tag{25}$$

$$\frac{\sigma_m^z(r, z)}{\sigma_a} = \alpha(1 + \gamma_1)Q_3 + \frac{(1 + \gamma_1)(Q_6 - \alpha Q_3)}{a^2 s_2}\left[b^2\ln\left(\frac{r}{a}\right) - \frac{r^2 - a^2}{2}\right]\frac{\cosh(\beta_3 z)}{\cosh(\beta_3 L)}\left\{-\alpha Q_3\right.$$
$$\left. + \frac{Q_5 + \alpha Q_3 - a^2\gamma s_1(1 + \nu_m)\beta_3^2 Q_3 Q_4}{a^2 s_2}\left[b^2\ln\left(\frac{r}{a}\right) - \frac{r^2 - a^2}{2}\right] + \gamma(1 + \nu_m)\beta_3^2 Q_3 Q_4\left[a^2\ln(r/a) - \frac{r^2 - a^2}{2}\right]\right\} \tag{26}$$

$$\frac{\sigma_c^z(r, z)}{\sigma_a} = \frac{(1 + \gamma_1)Q_6}{\alpha_1} + \frac{(1 + \gamma_1)Q_5}{\alpha_1}\frac{\cosh(\beta_3 z)}{\cosh(\beta_3 L)} + (1 + \gamma_1)\left\{\frac{\gamma_1(1 + \nu_c)(\alpha Q_3 - Q_6)}{\gamma s_1(1 + \nu_m)} + \left[a^2\gamma_1(1 + \nu_c)\beta_3^2\left(\frac{s_2}{s_1}\right)Q_3\right.\right.$$
$$\left.\left. - \frac{\gamma_1(1 + \nu_c)(\alpha Q_3 + Q_5)}{\gamma s_1(1 + \nu_m)}\right]\left[\frac{\cosh(\beta_3 z)}{\cosh(\beta_3 L)}\right]\right\}\left[\left(\frac{B}{b}\right)^2\ln(r/b) - \frac{r^2 - b^2}{2b^2}\right] \tag{27}$$

where the coefficients Q_4, Q_5 and Q_6 are given in Appendix 1. Similarly, the solutions for the interface shear stresses, normalized with the remotely applied stress, σ_a, are also obtained as

$$\frac{\tau_i(a, z)}{\sigma_a} = \frac{a(1 + \gamma_1)\beta_3 Q_3}{2}\frac{\sinh(\beta_3 z)}{\cosh(\beta_3 L)} \tag{28}$$

$$\frac{\tau_i(b, z)}{\sigma_a} = \frac{-a^2(1 + \gamma_1)\beta_3 Q_3 Q_4}{2b}\frac{\sinh(\beta_3 z)}{\cosh(\beta_3 L)} \tag{29}$$

By replacing $\tau_i(a, z)$ and $\tau_i(b, z)$ in Equations 11 and 12 by the solutions obtained in Equations 28 and 29, the shear stresses in the matrix and the composite medium can directly be calculated.

2.3. Fibre fragmentation criterion

The embedded fibre fractures when the stress applied to the composite at its remote ends is high enough to cause the maximum fibre axial stress to reach the local fibre tensile strength. Following Part I of this paper, (see also Appendix 2) an average strength theory based on the Weibull probability of failure [11] is employed here as the criterion of fibre fragmentation. Because the fibre axial stress is maximum at the fibre centre, $z = 0$, the fibre fractures if

$$\sigma_f^z(z)|_{z=0} = \sigma_{TS}(2L) = \sigma_{TS}(2L_g)\left(\frac{L}{L_g}\right)^{1/m} \tag{30}$$

where $\sigma_{TS}(2L_g)$ is the average strength of the fibre corresponding to a gauge length $2L_g$ and is given by

$$\sigma_{TS}(2L_g) = [\sigma_u(2L_g)]^{-1/m}\Gamma\left(1 + \frac{1}{m}\right) \tag{31}$$

Therefore, by substituting Equation 30 into the fibre axial stress given by Equation 25, the fibre fragmentation criterion is obtained in terms of the external stress applied at remote ends, $\sigma_a = \sigma_{af}$

$$\sigma_{af} = \frac{\sigma_{TS}}{(1 + \gamma_1)Q_3}\frac{\cosh(\beta_3 L)}{\cosh(\beta_3 L) - 1} \tag{32}$$

By rearranging Equation 32, the mean fibre fragment length is obtained as a function of the external stress, σ_{af}, and fibre tensile strength, $\sigma_{TS}(2L)$

$$2L = \left(\frac{2}{\beta_3}\right)\cosh^{-1}\left[\frac{(1 + \gamma_1)Q_3\sigma_{af}}{(1 + \gamma_1)Q_3\sigma_{af} - \sigma_{TS}(2L)}\right] \tag{33}$$

The fibre fragmentation criterion represented by Equation 32 is only valid when the interface is fully bonded. This means that the maximum fibre–matrix interface shear stress obtained at the fibre ends, $z = \pm L$, in Equation 28 must always be smaller than the interface shear bond strength, τ_b. Therefore, the condition for full bonding is expressed as a function of the materials properties, $\sigma_{TS}(2L)$ and τ_b, from Equations 28 and 32

$$\tau_b > \frac{a\beta_3}{2}\frac{\sinh(\beta_3 L)}{\cosh(\beta_3 L) - 1}\sigma_{TS}(2L) \tag{34}$$

2.4. Interface debond criterion

Based on the shear strength criterion, a debond crack initiates when the maximum interface shear stress reaches the shear bond strength, τ_b. Because the maximum interface shear stress occurs at the fibre ends, the interface debond criterion is obtained from Equation 28 in terms of applied stress at remote ends, $\sigma_a = \sigma_{ad}$

$$\sigma_{ad} = \frac{2\tau_b}{a(1 + \gamma_1)\beta_3 Q_3}\coth(\beta_3 L) \tag{35}$$

3. Results

Specific results are calculated to show the stress distributions as well as the characteristic fibre fragmentation and interface debond phenomena based on the solutions obtained in the preceding section for a model composite of carbon fibre–epoxy matrix [12]. Table 1 gives the mechanical properties of the composite constituents and the Weibull statistics of tensile strength of the fibre used in the present study. Unless otherwise specified, radii $a = 0.003$ mm and $B = 1.0$ mm for the fibre and the composite medium,

TABLE I Mechanical/interface properties of carbon fibre–epoxy matrix composites and the Weibull parameters of fibre tensile strength.

Mechanical	Interface properties	Weibull parameters for fibre tensile strength
$E_f = 230$ GPa	$\tau_b = 72.7$ MPa	$2L_g = 12$ mm
$E_m = 3.0$ GPa		$\sigma_{TS}(2L_g) = 2.35$ GPa
$\nu_f = 0.2$		$m = 3.8$
$\nu_m = 0.4$		$\sigma_u = 5.0$

respectively, and fibre length $2L = 2.0$ mm are used in the present calculation to show the essential trends. Examples of distributions of the axial and shear stresses are given along the fibre axis.

3.1. Stress distributions in the composite constituents

The general distributions of the fibre axial stress (FAS) and the fibre–matrix interface shear stresses (ISS) shown in Fig. 2 are very similar to those obtained from a single-fibre composite model. The FAS is maximum at the mid-length, and decreases towards zero at the fibre ends. It is interesting to note that an increase in fibre volume fraction, V_f, results in the central portion of the fibre with a constant plateau value becoming relatively longer while the stress gradient near the fibre ends being more drastic within a short distance (Fig. 2a). Therefore, the corresponding fibre–matrix interface shear stress (ISS) and the stress gradient gradually increase with a larger portion of the fibre central region being free of ISS (Fig. 2b). It is also noted that the matrix–composite interface shear stress (ISS) and the stress gradient decrease with increasing fibre V_f (Fig. 2c). When the fibre V_f is greater than about 0.3, the maximum ISS value for the matrix–composite interface obtained at the fibre ends tends to become negative.

The shear stresses, both at the matrix and the composite medium, increase exponentially with distance away from the fibre centre, as shown in Fig. 3. Also superimposed in these plots is the shear stress at the matrix–composite medium interface, $\tau_i(b, z)$, to show clearly the variation of the shear stresses in the radial direction across the interface. In contrast to the similar functional variation with respect to the axial distance, these shear stresses display reversed responses with respect to the radial distance. At a given axial position, the matrix shear stress increases gradually towards the matrix–composite medium interface (Fig. 3a), whereas the shear stress in the composite medium decreases dramatically towards the outermost surface of the composite cylinder. This is a direct reflection of the boundary conditions employed in the theoretical analysis.

The predominant effect of fibre volume fraction V_f, on the stress distributions is summarized in Fig. 4 where the characteristic maximum FAS and ISS values, obtained in the mid-fibre and fibre ends, respectively, are plotted as a function of fibre V_f.

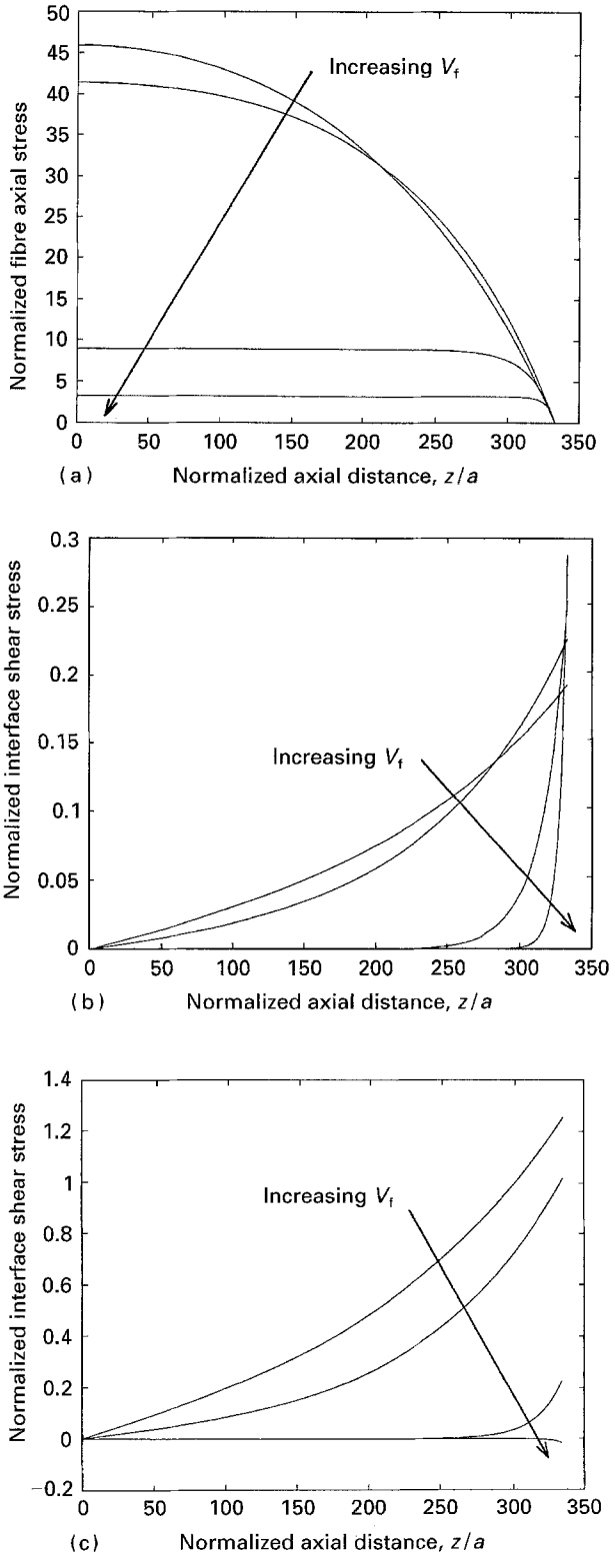

Figure 2 Distribution of (a) normalized fibre axial stress, σ_f^z/σ_a, (b) normalized fibre–matrix interface shear stress, $\tau_i(a, z)/\sigma_a$, and (c) normalized matrix–composite interface shear stress, $\tau_i(b, z)/\sigma_a$, along the fibre axis, z/a, for fibre volume fractions $V_f = 0.005$, 0.01, 0.1 and 0.3.

A completely reversed fibre V_f dependence is manifested between the FAS and the ISS (Fig. 4a and 4b). The maximum FAS decreases, whereas the maximum fibre–matrix ISS increases almost parabolically with increasing V_f. The principal effect of matrix Young's modulus, E_m, is seen to attenuate the effect of fibre volume fraction on these stress fields. In particular, the

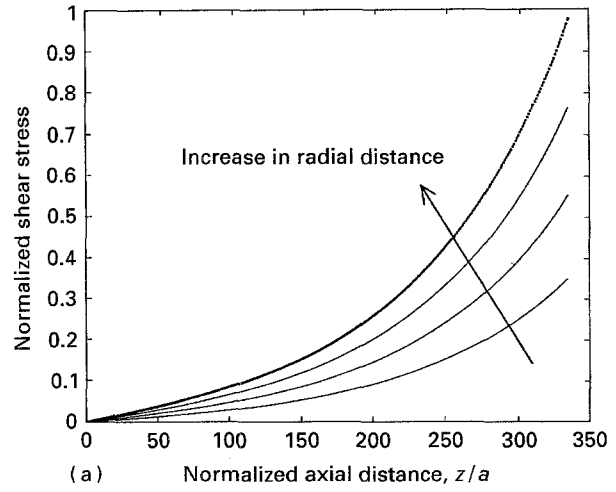

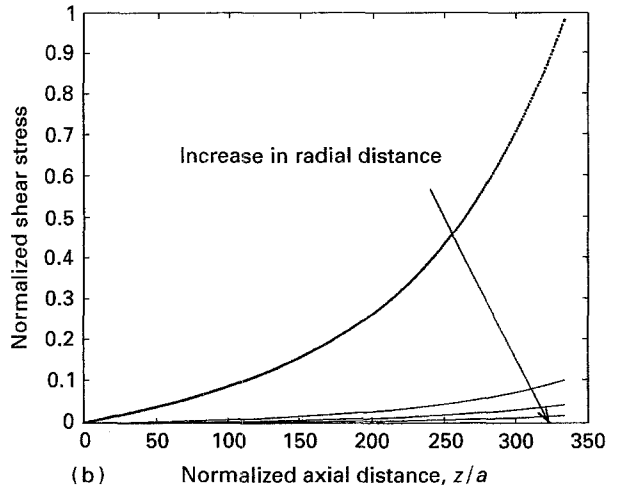

Figure 3 Distribution of (a) normalized shear stress, $\tau_m(r, z)/\sigma_a$, in the matrix for $r = a + (b - a)/4$, $a + (b - a)/2$, $a + 3(b - a)/4$ and (b) normalized shear stress, $\tau_c(r, z)/\sigma_a$, in the composite medium for $r = b$, $b + (B - b)/4$, $b + (B - b)/2$ and $b + 3(B - b)/4$, along the fibre axis, z/a.

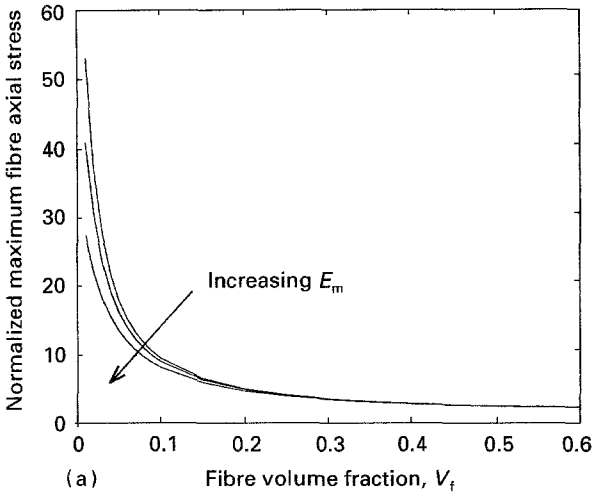

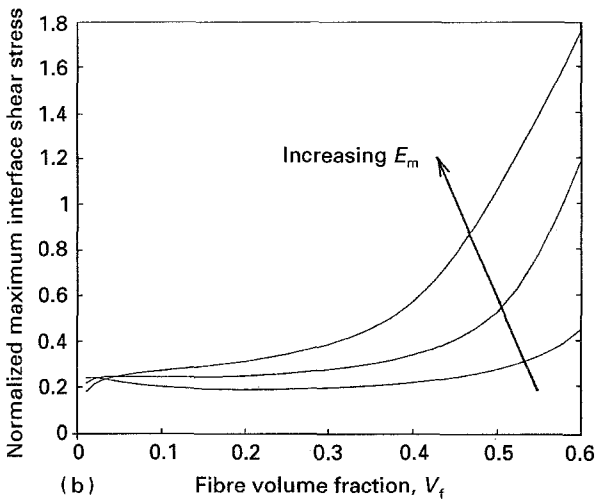

Figure 4 (a) Normalized maximum fibre axial stress, $[\sigma_f^z]_{max}/\sigma_a$, and (b) normalized maximum fibre–matrix interface shear stress, $[\tau_i(a, z)]_{max}/\sigma_a$, as a function of fibre volume fraction, for Young's moduli of matrix $E_m = 1.5$, 3.0 and 6.0 GPa.

effect of E_m becomes increasingly more important at a high V_f. In the case of ISS (Fig. 4b), this is thought to be associated with the reduced size of the matrix annulus surrounding the discontinuous, isolated fibre when V_f is increased. At the same time, an increase in V_f effectively increases the relative size of the average composite cylinder. From the functional viewpoints, the use of a high E_m is seen to have much the same effect as an increase in V_f. This is because both the factors increase the stiffness of the composite medium. As the Young's modulus of the fibre used in the calculation is already significantly greater than the matrix, the stiffening effect due to the use of a matrix material with a high Young's modulus is shown to be not significant as that due to the increase in V_f.

3.2. Fibre fragmentation and interface debond

The fibre fragmentation criterion specified by Equation (32) is shown in Fig. 5, in which the mean fibre fragment length, $2L$, is plotted as a function of applied strain, ε, at remote ends. It is noted that $2L$ declines instantaneously within a narrow range of applied

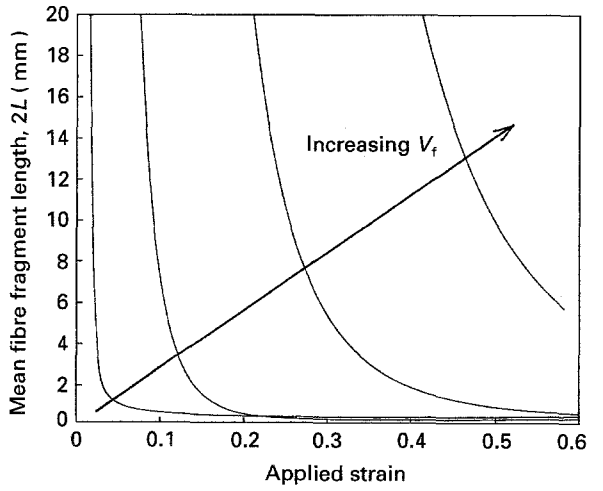

Figure 5 Variation of mean fibre fragment length, $2L$, as a function of applied strain, ε, for fibre volume fractions $V_f = 0.005$, 0.01, 0.1 and 0.3.

strain, for a low fibre V_f in particular. The precipitous drop in $2L$ is followed by an almost constant value with further increase in the applied strain for all fibre V_f studied. A composite with high fibre content certainly requires a significantly higher applied strain to

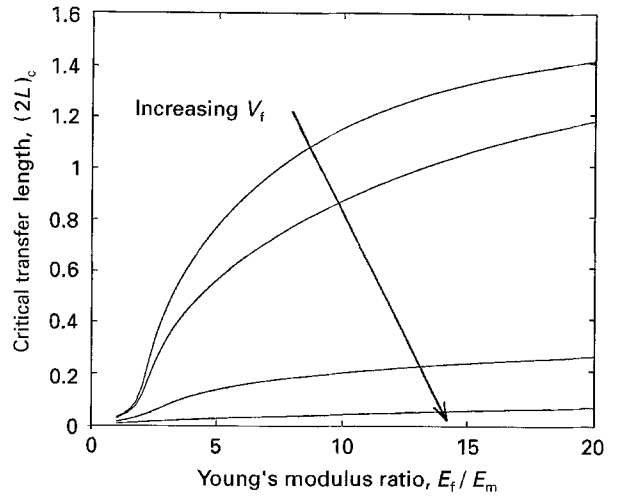

Figure 6 Variation of critical transfer length, $2L_c$, as a function of Young's modulus ratio of the fibre to the matrix, E_f/E_m, for fibre volume fractions $V_f = 0.005$, 0.01, 0.1 and 0.3.

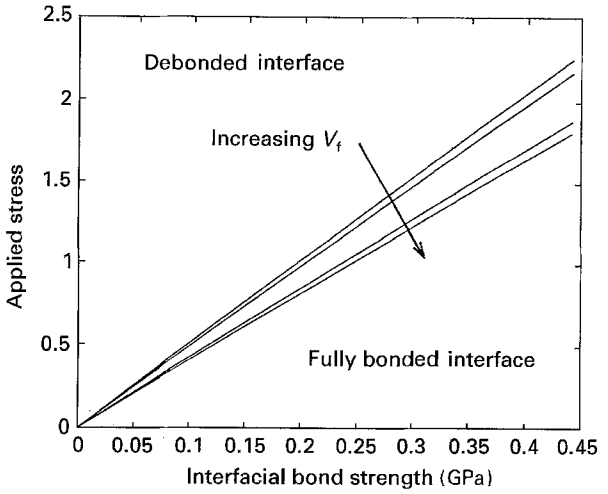

Figure 8 Plots of applied stresses required for interfacial debonding, σ_{ad}, as a function of interface shear bond strength, τ_b, calculated based on Equation 35, for fibre volume fractions $V_f = 0.005$, 0.01, 0.1 and 0.3.

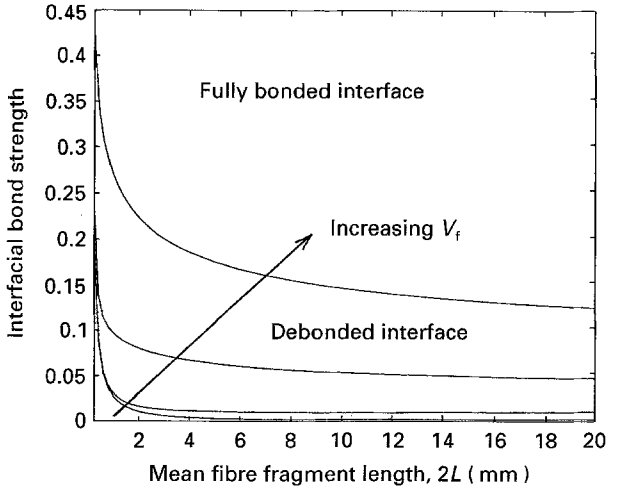

Figure 7 Plot of interface shear bond strength, τ_b, as a function of fibre length, $2L$, calculated based on Equation 34 for varied fibre volume fractions $V_f = 0.005$, 0.01, 0.1 and 0.3.

cause the fibres to break into given lengths. This result is considered consistent with the parabolic decrease in the maximum FAS with increase in fibre V_f shown in Fig. 4a. The dependence of critical transfer length, $(2L)_c$ on Young's modulus ratio, E_f/E_m, is presented in Fig. 6. The critical transfer length is defined here as the fibre length necessary to build up a maximum stress equal to 90% of that for an infinitely long fibre [13]. For a low fibre V_f, $(2L)_c$ surges rapidly with the modulus ratio, E_f/E_m, before its gradient becomes negligible at a high modulus ratio, whereas for a high fibre V_f, $(2L)_c$ increases only marginally for the whole range of modulus ratio studied. At a given modulus ratio, $(2L)_c$ varies inversely with fibre V_f.

Fig. 7 presents the critical combination of the interface shear bond strength, τ_b, and the fibre fragment length, $2L$, which satisfy the debond criterion at the fibre–matrix interface. The regions above and below the curves in Fig. 7 represent the fully bounded and partially debonded interfaces, respectively. Also envisaged from this figure is that with an increase in fibre V_f at a given fibre length, the relative area for debonded interface increases within the range of the variables studied. This, in turn, means that the fibre–matrix interfacial debonding becomes easier with increasing the fibre V_f. Finally, the interface debond criterion is depicted in Fig. 8 in terms of the applied stress, σ_{ad}, required for initial interfacial debonding according to Equation 35. The debond stress, σ_{ad}, varies linearly with the interface bond strength, τ_b. A high fibre V_f is shown to require a marginally lower applied stress for debonding at a given interfacial bond strength and fibre length, which agrees with the observation noted from Figs 3b and 7.

4. Discussion

In the light of the parametric study presented in the foregoing section, the implications of the present theoretical analysis can be summarized with regard to the fibre fragmentation and interfacial debonding phenomena. The higher the fibre volume fraction, V_f, and the Young's modulus of the matrix, E_m, the higher is the required external stress to allow the maximum FAS to reach the local fibre tensile strength. In other words, from the practical viewpoint of the fibre fragmentation test, a higher applied strain is required to obtain the identical mean fibre fragment length, $2L$, with increasing V_f. However, the same condition results in a higher maximum fibre–matrix ISS. It seems that the concentration of ISS at the fibre ends is promoted by the boundary condition used in the theoretical analysis that the cross-sectional ends are assumed unbonded. The result indicates that debond initiation becomes increasingly easier with increasing stiffness of the composite medium as a result of high fibre V_f and matrix Young's modulus, E_m. It is expected that once the interface debond crack initiates, its propagation requires a higher external stress because of softening of the composite medium that the interfacial debond may cause.

Further implications can be made of the foregoing accounts with regard to the fracture modes of composites containing aligned discontinuous fibres

embedded in a brittle matrix. When V_f and E_m are low, the failure of the composite is likely to be caused by the damage process accumulated by the fibre fracture which is rather catastrophic without much debonding and/or delamination. For a composite with high V_f and E_m the failure tends to be more stable and progressive due to the large energy absorbed during interfacial debond/delamination. Certainly, the occurrence of these two opposing fracture phenomena, the so-called transverse fracture versus longitudinal splitting, is strongly dependent on the relative magnitudes of characteristic strength properties of the composite constituents. The most important properties are identified to be the tensile strength of the fibre, σ_{TS}, and the interfacial shear bond strength, τ_b, as the criteria for fibre fracture and interface debonding derived in Section 2 suggest. Alternatively, the transition between these fracture phenomena can be expressed by two characteristic fracture properties, namely the fracture toughness for transverse fracture, G_T, and the fracture toughness of the fibre–matrix (or laminar) interface, G_L. Depending on the criteria and the assumptions used, the toughness ratio is reported $G_T/G_L \approx 0.12$ [14, 15] or 0.25 [16], for transition of fracture modes in a unidirectional continuous fibre composite.

The discussion presented above is based on the assumptions made in the analysis that the Young's modulus of the composite medium, E_c, varies only with the Young's moduli and volume fractions of the composite constituents. However, it is envisaged that for practical composites containing discontinuous aligned fibres, damage developed during loading in the form of fibre fracture, matrix cracking and interfacial debonding may degrade the composite mechanical properties. In particular, the interfacial debonding would result in significant reduction in strengths under both longitudinal tension and compression, as well as in transverse tension. Nevertheless, it is expected that the Young's modulus of a composite will remain almost unchanged even with interface debonding, as evinced in a recent report [17] on the roles of interfacial adhesion on the mechanical properties of carbon fibre–epoxy matrix composites. Regarding the effects of fragmentation of the fibres in a composite medium, the composite longitudinal strength would gradually decreases with the shortening of fibre length, as for the average stress felt by the fibres. However, the Young's modulus of the composite is little influenced by the fibre length as long as its aspect ratio, L/a, is sufficiently large, say larger than about 100 [18], which is the case of the carbon fibre–epoxy matrix composites studied in the present paper.

5. Conclusion

The stress transfer in a multiple fibre composite, which was subjected to a uniaxial tension, was studied. Special emphasis was placed on the effects of interactions between reinforcing fibres for varying fibre volume fraction and matrix Young's modulus. Solutions have been derived for the stress components in the three-cylinder composite model. Criteria for two opposing fracture phenomena, namely the fibre fragmentation and fibre–matrix interface debonding, were also established for the loading geometry considered. A parametric study for a model composite of carbon fibre–epoxy matrix composite suggests that the fibre fragmentation becomes increasingly difficult while the interfacial debonding becomes easier with increasing stiffness of the average composite medium surrounding the core single-fibre composite. This observation has an implication for aligned discontinuous fibre composites in that the stability and the energy absorption capability of fracture process can be enhanced by increasing the fibre volume fraction and the matrix Young's modulus.

Acknowledgements

The authors thank the Australian Research Council (ARC) for continuing support of the project on engineered composite interfaces. A special thanks are due to Mr A.D. Garnadi for the calculation and plotting of the figures. Part of the paper was presented at the first International Conference on Composite Engineering (ICCE-1, New Orleans, USA, August 1994).

Appendix 1. Non-dimensional Coefficients Q_1, Q_2, Q_3, Q_4, Q_5 and Q_6

$$Q_1 = \left[T_4\left(1+\frac{s_2}{s_1}\right) + (T_4 - T_3)\left(\frac{\alpha}{\gamma} - \frac{s_3}{s_1}\right) + T_2 T_5 \right] \Big/ \left(T_1 T_4 + \frac{s_3}{s_1} T_2 \right) + \left(\frac{a}{b}\right)^2 \left(- T_1 T_5 + \frac{s_2 s_3}{s_1^2} \right) \Big/ \left(T_1 T_4 + \frac{s_3}{s_1} T_2 \right) \tag{A1}$$

$$Q_2 = - T_5 \left\{ \left(\frac{a}{b}\right)^2 \left[\alpha \frac{s_3}{s_1} + 1 + \frac{\alpha}{\gamma} - \frac{s_3}{s_1} \right] + T_3 + \alpha T_4 \right\} \Big/ \left(T_1 T_4 + \frac{s_3}{s_1} T_2 \right) \tag{A2}$$

$$Q_3 = \left(\frac{B}{b}\right)^2 T_5 \Big/ \left[Q_2 \left(T_1 T_4 + \frac{s_3}{s_1} T_2 \right) \right] \tag{A3}$$

$$Q_4 = \left\{ b^2 \beta_3^2 \left(T_1 T_4 + \frac{s_3}{s_1} T_2 \right) + \left(\frac{b}{a}\right)^2 \times \left[T_4 \left(1 + \frac{\alpha}{\gamma} - \frac{s_3}{s_1} \right) - \frac{s_3}{s_1} T_3 \right] \right\} \Big/ \left[\frac{s_3}{s_1} + \left(\frac{b}{a}\right)^2 T_4 \right] \tag{A4}$$

$$Q_5 = Q_3 \left\{ a^2 \beta_3^2 \left[T_1 - \left(\frac{b}{a}\right)^2 T_2 \right] + \left[1 + \frac{\alpha}{\gamma} - \frac{s_3}{s_1} + \left(\frac{b}{a}\right)^2 T_3 \right] \right\} \left[\frac{s_3}{s_1} + \left(\frac{b}{a}\right)^2 T_4 \right] \tag{A5}$$

$$Q_6 = \left\{ \left(\frac{B}{a}\right)^2 - Q_3 \left[1 + \frac{\alpha}{\gamma} - \frac{s_3}{s_1} + \left(\frac{b}{a}\right)^2 T_3 \right] \right\} \Big/ \left[\frac{s_3}{s_1} + \left(\frac{b}{a}\right)^2 T_4 \right] \tag{A6}$$

where

$$s_1 = \ln\left(\frac{b}{a}\right) - \frac{1}{2\gamma} \quad \text{(A7)}$$

$$s_2 = \left(\frac{b}{a}\right)^2 \ln\left(\frac{b}{a}\right) - \frac{1}{2\gamma} \quad \text{(A8)}$$

$$s_3 = \left(\frac{b}{a}\right)^2 \ln\left(\frac{b}{a}\right) - \frac{1+2\gamma}{4\gamma^2} \quad \text{(A9)}$$

$$s_4 = \left(\frac{b}{a}\right)^4 \ln\left(\frac{b}{a}\right) - \frac{3+2\gamma}{4\gamma^2} \quad \text{(A10)}$$

$$s_5 = \left(\frac{B}{a}\right)^2 \ln\left(\frac{B}{a}\right) - \frac{1}{2\gamma_1} \quad \text{(A11)}$$

$$s_6 = \left(\frac{B}{b}\right)^4 \ln\left(\frac{B}{b}\right) - \frac{3+2\gamma_1}{4\gamma_1^2} \quad \text{(A12)}$$

$$T_1 = \gamma(1+\nu_m)\frac{s_2 s_3 - s_1 s_4}{s_1} \quad \text{(A13)}$$

$$T_2 = \gamma_1(1+\nu_c)\frac{s_2 s_6}{s_1} \quad \text{(A14)}$$

$$T_3 = \frac{\alpha\gamma_1(1+\nu_c)s_6}{\gamma(1+\nu_m)s_1} \quad \text{(A15)}$$

$$T_4 = \frac{\gamma(1+\nu_m)s_1 - \alpha_1\gamma_1^2(1+\nu_c)s_6}{\alpha_1\gamma\gamma_1(1+\nu_m)s_1} \quad \text{(A16)}$$

$$T_5 = \frac{1}{\gamma(1+\nu_m)s_1} \quad \text{(A17)}$$

Appendix 2. Correction of typographic errors in Part 1 of this paper [6]

Equation 3 should read

$$\beta_z^2 = \frac{(b^2-a^2)(1+\alpha/Y)}{(1+\nu_m)[b^4\ln(b/a) - (b^2-a^2)^2/2 - (b^4-a^4)/4.]} \quad (3)$$

and equations 12 and 13 should read

$$m_1 = \frac{-B_1 + (B_1^2 + 4\lambda B_1)^{\frac{1}{2}}}{2} \quad (12)$$

$$m_2 = \frac{-B_1 + (B_1^2 + 4\lambda B_1)^{\frac{1}{2}}}{2} \quad (13)$$

Equation 36 should read

$$\tau_b < \frac{a\beta_2}{a} \frac{[n_3 + \nu_m n_1(\alpha+\gamma)]\sigma_{TS}(2L) + \alpha\nu_f(n_1+\lambda)\bar{\sigma}}{n_3\coth[\beta_2(L-l)] - [n_3+\nu_m n_1(\alpha+\gamma)]\operatorname{cosech}[\beta_2(L-l)]} \quad (36)$$

and Equation A10 should read

$$\sigma_m^z(b,z) = \sigma_f^z(z)\left[\alpha - \frac{1}{\beta_1^2\gamma} - \frac{\alpha}{(\beta_1\gamma)^2}\right] + \sigma\frac{1+\gamma}{(\beta_1\gamma)^2} \quad \text{(A10)}$$

References

1. A. KELLY and W. R. TYSON, *J. Mech. Phys. Solids* **13** (1965) 329.
2. J. K. KIM and Y. W. MAI, in "Structure and Properties of Fibre Composites", Materials Science and Technology Series, Vol. 13, edited by T. W. Chou (VCH, Weinheim, Germany, 1993) pp. 239–89.
3. P. FEILLARD, G. DESARMOT and J. P. FAVRE, *Compos. Sci. Technol.* **50** (1994) 265.
4. J. K. KIM, L. M. ZHOU and Y. W. MAI, in "Handbook of Advanced Materials Testing", edited by N. P. Cheremisinoff (Marcel Dekker, New York, 1994) pp. 327–66.
5. H. L. COX, *Br. J. Appl. Phys.* **3** (1952) 72.
6. J. K. KIM, L. M. ZHOU and Y. W. MAI, *J. Mater. Sci.* **28** (1993) 6233.
7. J. K. KIM, S. V. LU and Y. W. MAI, *ibid.* **29** (1994) 554.
8. J. K. KIM, L. M. ZHOU, S. J. BRYAN and Y. W. MAI, *Composites* **25** (1994) 470.
9. C. H. HSUEH, *Mater. Sci. Eng.* **A 165** (1993) 189.
10. L. N. McCARTNEY, *Proc. R. Soc. Lond.* **A 425** (1989) 215.
11. S. VAN DER ZWAAG, *J. Test. Eval. (JTEVA)* **17** (1989) 292.
12. L. M. ZHOU, J. K. KIM, C. A. BAILLIE and Y. W. MAI, *J. Compos. Mater.* **29** (1995) in press.
13. B. W. ROSEN, *AIAA J.* **2** (1964) 1985.
14. K. KENDALL, Proc. R. Soc. Lond. **A 344** (1975) 287.
15. J. A. NAIRN, *J. Reinf. Plast. Compos.* **9** (1990) 91.
16. A. G. EVANS and D. B. MARSHALL, *Acta Metall.* **37** (1989) 2567.
17. L. T. DRZAL and M. MADHUKAR, *J. Mater. Sci.* **28** (1993) 569.
18. S. NOMURA and T. W. CHOU, *J. Appl. Mech.* **51** (1984) 540.

Received 3 November 1994
and accepted 20 January 1995